ISSN (e): 2250 – 3005 || Volume, 06 || Issue, 12|| December – 2016 ||
International Journal of Computational Engineering Research (IJCER)

Alternative and Explicit Derivation of the Lattice Boltzmann Equation for the Unsteady Incompressible Navier-Stokes Equation

John Ryan Murdock[1,a] Song-Lin Yang[1,] Professor [b]
[1]Department of Mechanical Engineering-Engineering Mechanics, Michigan Technological University, Houghton, MI 49931

ABSTRACT
A lattice Boltzmann equation for fully incompressible flows is derived through the utilization of appropriate ansatzes. The result is a singular equilibrium distribution function which clarifies the algorithm for general implementation, and ensures correct steady and unsteady behavior. Through the Chapman-Enskog expansion, the exact incompressible Navier-Stokes equations are recovered. With 2D and 3D canonical numerical simulations, the application, accuracy, and workable boundary conditions are shown. Several unique benefits over the standard equation and alternative forms presented in literature are found, including faster convergence rate and greater stability.

Keywords: *Ansatz method, Chapman-Enskog expansion, equilibrium distribution function, incompressible flow, lattice Boltzmann method, unsteady flow*

I. INTRODUCTION

While the lattice Boltzmann equation (LBE) is frequently applied to incompressible flows, the standard form actually recovers the compressible Navier-Stokes (N-S) equations in the low Mach number limit. He et al. [1] suggest that the standard LBE can be viewed as an artificial compressibility method, with the resultant numerical error. To eliminate this error several steps toward a truly incompressible LBE exist in the literature [2-6]. Although limiting density variation most schemes [2-5] do not recover the exactly incompressible conservation equations:

$$\nabla \cdot \boldsymbol{u} = 0, \tag{1}$$

$$\frac{\partial \boldsymbol{u}}{\partial t} + \nabla \cdot (\boldsymbol{u}\boldsymbol{u}) = -\frac{1}{\rho_0}\nabla P + \nu \nabla^2 \boldsymbol{u}. \tag{2}$$

Additionally, with the exception of He and Luo [5] and Guo et al. [6], the proposed schemes are not designed for transient flows. The He and Luo [5] scheme recovers the artificial compressibility N-S equations, which further requires that the characteristic time be large relative to the characteristic length.
Guo et al. [6] design a fully capable unsteady incompressible scheme with three free parameters present in the definition of the D2Q9 equilibrium distribution function (EDF),

$$f_a^{eq} = \begin{cases} -4\sigma P/c^2 + S_a(\boldsymbol{u}), & a = 0 \\ \lambda P/c^2 + S_a(\boldsymbol{u}), & a = 1,2,3,4 \\ \gamma P/c^2 + S_a(\boldsymbol{u}), & a = 5,6,7,8 \end{cases} \tag{3}$$

where

$$S_a(\boldsymbol{u}) = w_a \left[3\frac{(\boldsymbol{e}_a \cdot \boldsymbol{u})}{c} + 4.5\frac{(\boldsymbol{e}_a \cdot \boldsymbol{u})^2}{c^2} - 1.5\frac{(\boldsymbol{u} \cdot \boldsymbol{u})}{c^2} \right], \tag{4}$$

These three parameters are governed by two equations,

$$\lambda + \gamma = \sigma, \qquad 2\lambda + 4\gamma = 1, \tag{5}$$

which create an infinite number of choices. Banda et al. [7] noted that while σ = 5/12, λ = 1/3, and γ = 1/12 are the parameters for the numerical tests in Guo et al.'s paper, questions exist about the properties of alternate possibilities. Shi et al. [8] utilize the same set of parameters to produce good results, however the choice is not explained or derived, nor is there an exploration of the alternative parameter choices from Guo et al.'s paper.
Questions from past literature, our research group, and those who implement code still exist about the uniqueness of the incompressible form, derivation techniques, and the merits of the alternate values for the parameters σ, λ, and γ. In this work we seek to build off of the work by Guo et al. to:

- Describe a general derivation process;
- Clarify the literature and parameters for those implementing the algorithm;
- Ensure consistent correct solutions;
- Evaluate the benefits to accuracy and stability with such a form.

This paper is organized as follows: Section 2 introduces the standard LBE and the derivation of a fully incompressible form through an appropriate ansatz. Section 3 presents numerical results which validate the form derived in section 2, compares results with other schemes, and explores the properties of alternate parameter values to equation 3. After the summary of section 4, the appendix shows the recovery of the incompressible N-S equations through the Chapman-Enskog expansion.

II. DERIVATION OF THE D2Q9 INCOMPRESSIBLE LBE

2.1. Standard LBE form

From the standard LBE,

$$f_a(\boldsymbol{x} + \delta\boldsymbol{x}, t + \delta t) = f_a(\boldsymbol{x}, t) - \frac{1}{\tau}\left(f_a(\boldsymbol{x}, t) - f_a^{eq}(\boldsymbol{x}, t)\right) \tag{6}$$

the Chapman-Enskog multiscale expansion, as detailed by Qian et al. [9], results in the mass and momentum conservation equations:

$$\frac{\partial \rho}{\partial t} + \nabla \cdot (\rho \boldsymbol{u}) = 0, \tag{7}$$

$$\frac{\partial (\rho \boldsymbol{u})}{\partial t} + \nabla \cdot (\rho \boldsymbol{u}\boldsymbol{u}) = -\nabla P + \nu\left(\nabla^2(\rho \boldsymbol{u}) + \nabla\left[\nabla \cdot (\rho \boldsymbol{u})\right]\right). \tag{8}$$

In the D2Q9 LBE

$$\rho = \sum_a f_a, \quad \rho \boldsymbol{u} = \sum_a c\boldsymbol{e}_a f_a, \quad c_s = \frac{c}{\sqrt{3}}, \quad P = c_s^2 \rho, \quad \nu = c_s^2\left(\tau - \frac{1}{2}\right)\delta t, \tag{9}$$

where $c = \delta x/\delta t$ is the lattice velocity, c_s is the speed of sound, $\boldsymbol{e}_a$ are the velocity vectors, and τ is the single collision relaxation time of the BGK model.
Many of the terms in equations 7 and 8 involve a variation of density with time or space, and thus suffer from compressibility error unlike the desired incompressible equations, 1 and 2. Relationships of equations set 9 depend on a speed of sound, and pressure an viscosity depend on that of sound.

2.2. An incompressible LBE derivation

An EDF must satisfy the necessary tensor symmetry and adhere to the incompressible conservation principles. For a valid EDF the form is first established, the governing principles are dictated, and an appropriate method is adopted to satisfy the form and principles. The result can be mathematically verified with the Chapman-Enskog expansion, shown in the appendix.
Based on the Maxwellian distribution and the nonlinearity of the momentum equation, an ansatz for the EDF form pertaining to the lattice discretization of figure 1 is established as:

$$f_a^{eq} = A_i + B_i(\boldsymbol{e}_a \cdot \boldsymbol{u}) + C_i(\boldsymbol{e}_a \cdot \boldsymbol{u})^2 + D_i(\boldsymbol{u} \cdot \boldsymbol{u}), \tag{10}$$

$$i = \begin{cases} 0 & \text{for } a = 0 \\ 1 & \text{for } a = 1,2,3,4 \\ 2 & \text{for } a = 5,6,7,8 \end{cases} \tag{11}$$

and as in Guo et al. [6] the mass and momentum governing principles are dictated as:

$$\sum_{a=0}^{8} f_a^{eq} = \sum_{a=0}^{8} f_a = Constant, \tag{12}$$

$$\sum_{a=0}^{8} \boldsymbol{ce}_a f_a^{eq} = \sum_{a=0}^{8} \boldsymbol{ce}_a f_a = \boldsymbol{u}, \tag{13}$$

and the zeroth-order incompressible momentum flux tensor is stated here as

$$\sum_{a=0}^{8} \boldsymbol{ce}_a \boldsymbol{ce}_a f_a^{eq} = \sum_{a=0}^{8} \boldsymbol{ce}_a \boldsymbol{ce}_a f_a = \frac{P}{\rho_0}\boldsymbol{I} + \boldsymbol{uu}. \tag{14}$$

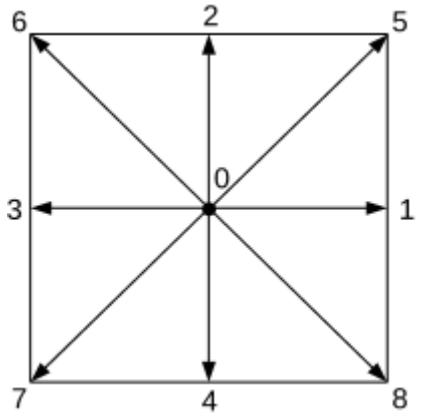

Figure 1. D2Q9 lattice velocities (*a*).

For generality and intuitive understanding we set *Constant* = 1 in the derivation. The additional assignment of *Constant* = 0, as in Guo et al. [6], is verified numerically to produce the identical result in section 3.

Remark 1: Equation 12 is critical in enforcing the zero-divergence law of equation 1. To validate that the statement made in equation 12 satisifies the requirement at each time step and point, both the summation of f_a and the finite difference method are independently evaulated in section 3.2. Both show adherence to zero velocity divergence.

There are 12 unknowns in equation 10,

$$\begin{array}{ccc} A_0 & A_1 & A_2 \\ B_0 & B_1 & B_2 \\ C_0 & C_1 & C_2 \\ D_0 & D_1 & D_2 \end{array}$$

Several of these parameters can be determined through the conservation equations and discrete lattice velocities. Due to the rest particle ($\boldsymbol{e}_0 = 0$),

$$B_0 = C_0 = 0, \tag{15}$$

and from the conservation principles 12 and 13,

$$\sum_{a=0}^{8} f_a^{eq} = A_0 + 4A_1 + 4A_2 + (2C_1 + 4C_2 + D_0 + 4D_1 + 4D_2)(\boldsymbol{u} \cdot \boldsymbol{u}) = 1, \tag{16}$$

$$\sum_{a=0}^{8} \boldsymbol{ce}_a f_a^{eq} = (2B_1 + 4B_2)c\boldsymbol{u} = \boldsymbol{u}. \tag{17}$$

Subsequently,

Through the 0th order momentum flux tensor, and in the 2D case $\underline{\mathbf{u}} = ui + vj$,

$$C_1 = \frac{1}{2c^2}, \qquad C_2 = \frac{1}{8c^2}, \tag{21}$$

which further defines,

$$\begin{gathered} D_0 + 4D_1 + 4D_2 = -2C_1 - 4C_2 = -\frac{3}{2c^2}, \quad c^2(2A_1 + 4A_2) = \frac{p}{\rho_0}, \\ 2D_1 + 4D_2 = -4C_2 = -\frac{1}{2c^2}. \end{gathered} \tag{22}$$

There are now 8 remaining unknowns, and only 5 linear equations. To provide an additional restriction an ansatz is introduced,

$$\frac{A_1}{A_2} = \frac{B_1}{B_2} = \frac{D_0}{D_1} = \frac{D_1}{D_2} = r. \tag{23}$$

Through a quadratic equation for *r* based on the relationships defined previously,

$$\begin{gathered} A_0 = 1 - \frac{2r+2}{c^2(r+2)}\frac{p}{\rho_0}, \; A_1 = \frac{r}{c^2(2r+4)}\frac{p}{\rho_0}, \; A_2 = \frac{1}{c^2(2r+4)}\frac{p}{\rho_0}, \\ B_1 = \frac{r}{c(2r+4)}, \; B_2 = \frac{1}{c(2r+4)}, \\ D_0 = -\frac{r}{c^2(r+2)}, \; D_1 = -\frac{1}{c^2(r+2)}, \; D_2 = -\frac{r-2}{c^2(8r+16)}. \end{gathered} \tag{24}$$

Consequently, *r* = 4, -2. 4 is the sensible result, and all of the unknowns can be resolved,

$$\begin{gathered} A_0 = 1 - \frac{5}{3c^2}\frac{p}{\rho_0}, \; A_1 = \frac{1}{3c^2}\frac{p}{\rho_0}, \; A_2 = \frac{1}{12c^2}\frac{p}{\rho_0}, \\ B_0 = 0, \; B_1 = \frac{1}{3c}, \; B_2 = \frac{1}{12c}, \\ C_0 = 0, \; C_1 = \frac{1}{2c^2}, \; C_2 = \frac{1}{8c^2}, \\ D_0 = -\frac{2}{3c^2}, \; D_1 = -\frac{1}{6c^2}, \; D_2 = -\frac{1}{24c^2} \end{gathered} \tag{25}$$

Building the EDF, the final incompressible form arises,

$$f_a^{eq} = \begin{cases} 1 - 5P/3c^2 + S_a(\boldsymbol{u}), & a = 0 \\ P/3c^2 + S_a(\boldsymbol{u}), & a = 1,2,3,4 \\ P/12c^2 + S_a(\boldsymbol{u}), & a = 5,6,7,8 \end{cases} \tag{26}$$

where

$$S_a(\boldsymbol{u}) = w_a \left[3\frac{(\boldsymbol{e}_a \cdot \boldsymbol{u})}{c} + \frac{9}{2}\frac{(\boldsymbol{e}_a \cdot \boldsymbol{u})^2}{c^2} - \frac{3}{2}\frac{(\boldsymbol{u} \cdot \boldsymbol{u})}{c^2} \right], \tag{27}$$

and the weights are those of the standard LBE,

$$w_a = \begin{cases} 4/9, & a = 0 \\ 1/9, & a = 1,2,3,4 \\ 1/36, & a = 5,6,7,8 \end{cases}$$

Based on the rest particle EDF of equation 26 the pressure is defined by

$$P = -\frac{c^2}{5}\left[\frac{2}{c^2}(\boldsymbol{u} \cdot \boldsymbol{u}) + 3f_0^{eq} + 3 \right], \tag{28}$$

a function of velocity squared. The Chapman-Enskog expansion detailed in the appendix yields a viscosity $\nu = c^2/3\,(\tau - 0.5)\delta t$ as well as the incompressible mass and momentum equations 1 and 2.

Remark 2: If we replace *Constant* = 1 with *Constant* = 0, the "1" is replaced by "0" in the $a = 0$ term in equation 26. Subsequently the "3" is replaced by "0" in equation 28. This pattern holds for other *Constant* assignments. As predicted, the numerical result is the same, as verified in section 3.

2.3. Discussion and comparison

The above derivation, combined with the Chapman-Enskog expansion of the appendix, has resolved several objectives of this study:

- An unambiguous EDF results;
- There is no speed of sound equation in the model, hence no need to have an equation of state for pressure and density;
- Clarity and rationale is established for the form of the EDF;
- The derivation is broadly applicable to other dimensions and lattice discretizations;
- Compressibility effects are eliminated and the model is valid for transient flows.

It is important to note that the form arrived at through this alternative approach satisfies equations 5 from Guo et al. [6]. However, other parameter values valid in equations 5 do not result from the ansatz approach taken here. In the next section, we show that these other parameter values are not favorable, and it is the form found in equation 26 that produces consistently valid results.

III. NUMERICAL RESULTS

Developing channel flow, the lid driven cavity (2D and 3D), Womersley flow, and the backward facing step serve as validation and verification tools for the form derived in the previous section. Wall boundary conditions are implemented with the halfway bounceback scheme, evaluated in He et al. [10]. Velocity inlets and moving walls are based on the revised halfway bounceback scheme of Ladd [11], where the momentum product is replaced by the form of momentum conservation of equation 2. Pressure boundaries are implemented with Chen's extrapolation scheme [12]. Prescribed velocities are 0.1 in LB units to stay within the low *Ma* limit.

Additionally, alternative parameters satisfying equation set 5 are implemented and evaluated. The evaluated sets ($\{\sigma,\lambda,\gamma\}$) are:

$$G1 = \{3/8, 1/4, 1/8\};$$

$$G2 = \{9/20, 2/5, 1/20\};$$

$$G3 = \{7/12, 2/3, -1/12\}.$$

The work of Banda et al. [7] was also considered. In their D2Q8 stability analysis they suggest a different parametric condition from Guo et al. [6], $\lambda = 4\gamma$. While appropriate for the 8-velocity lattice, the condition lacks generality, and quickly becomes unstable in our numerical tests. The D2Q9 EDF is no longer valid when the incompressible mass conservation principle is applied. However, the conditions presented were not designed to resolve the exact objectives we resolve in this work.

Results are found which are in line with those found by Guo et al. [6]. This is to be expected as the boundary condition impelementation is one of the few differences, and the form derived here holds the same values as Guo et al. [6] chose to employ in their numerical tests.

3.1. Developing channel flow

A uniform inlet velocity is applied on the left side of the domain, and exits three channel heights to the right. No slip walls are applied to the top and bottom infinite parallel plates. Since the length of the channel exceeds the estimated entrance length for the simulated $Re = 10$, the simulation has a simply analytic solution from White [13]: $u_x(x,H/2)=1.5\,u_{in}$. The simplicity of the flow makes it a good test of the alternate sets, *G*1-3, as well as the order of accuracy of the method. A root mean square (RMS) residual of 5e-15 is achieved.

In table 1, the form derived in this work results in valid solutions while alternates result in fatal instabilities. The maximum *x*-velocity is in good agreement with the analytic solution, the maximum *y*-velocity at all grids is machine zero.

A brief look at the results in figure 2 shows second order accuracy, in keeping with the standard LBE evaluated by Meng and Zhang [14].

Figure 3 displays convergence history in the standard and incompressible LBE to demonstrate improved simulation speed in the form of the present work. For developing channel flow on a 27x9 grid the incompressible scheme achieves the convergence criterion with about 15% fewer steps. This behavior is somewhat analogous to the preconditioned LBE of Guo et al. [15], but not limited to steady flows. Additionally, for the given grid and boundary conditions the error of the standard LBE is 1.002% where the incompressible form has an error two orders of magnitude smaller.

Table 1. Maximum non-dimensional velocity and analytic error in developing channel flow.
***Indicates fatal instability.**

Grid	**Present Work**		**G1**		**G2**		**G3**	
	u_{max}	% Err	u_{max}	% Err	u_{max}	% Err	u_{max}	% Err
9x3	1.4841	1.057	1.4868	0.8784	1.4839	1.075	*	*
15x5	1.5070	0.4670	1.5179	1.192	1.5033	0.2214	*	*
21x7	1.5005	0.03580	1.5064	0.4247	1.4987	0.08547	*	*
27x9	1.4998	0.01653	1.5055	0.3684	1.4982	0.1221	*	*

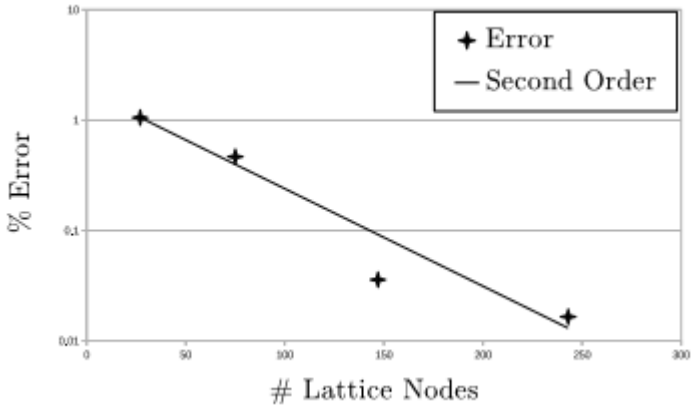

Figure 2. Developing channel flow convergence of u_{max} error with node count.

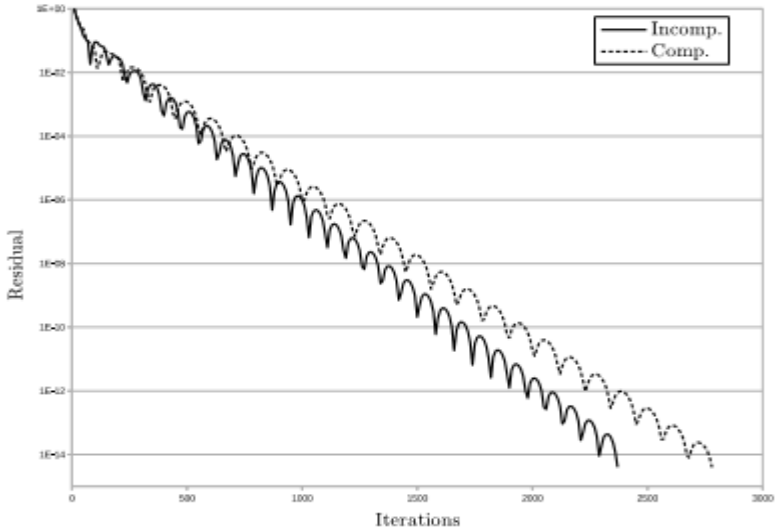

Figure 3. Developing channel flow residual history of standard and incompressible LBEs.

3.2. Lid driven cavity

Incompressible flow in the lid driven cavity is well documented in literature. The geometry is simple, with only the top wall moving and all boundaries no slip flat walls. However, complex flow patterns form. *Re* = 100, 400, 1000 are compared against the work of Marchi et al. [16].The alternate parameter values *G*1-3 are again attempted. The grid is 257x257 and convergence is taken to RMS 1e-9.

Table 2 displays the reference values for comparison, table 3 and 4 display results for the present work and the first alternative set *G*1, respectively. G2-3 results are not presented because both proved fatally unstable at every *Re*. This indicates that as parameters approach those presented in this work, the solution comes closer to a proper incompressible form.The results of table 3 and figures 4/5 show excellent agreement with higher grid results from literature. For this grid, stable simulations exist to *Re* 5000 while the standard LBE quickly becomes fatally unstable at the same *Re*.

An additional important point is made in this numerical test: the LBE derived in this work satisfies the zero velocity divergence requirement ($\partial_x \boldsymbol{u} = 0$). The finite difference method is applied to each node at each time step. A second-order central differencing is performed on the interior nodes, and a second-order backward differencing scheme on the boundary nodes. To within numerical error, the zero-divergence requirement is well

satisfied.In this simulation both *Constant* = 0 and 1 have been utilized. The results are identical at every decimal place, as expected. It is only critical that a constant value is used, and the derivation is consistent throughout.

Table 2. Reference values from Marchi et al. [16] lid driven cavity study.

Re	u_x	u_y	$\|\|\boldsymbol{u}\|\|$
100	-2.0915e-1	5.7537e-2	2.1692e-1
400	-1.1505e-1	5.2058e-2	1.2628e-1
1000	-6.2056e-2	2.5799e-2	6.7205e-2

Table 3. Present work center point values of lid driven cavity with velocity magnitude variance from [16].

Re	**Present Work**			
	u_x	u_y	$\|\|\boldsymbol{u}\|\|$	% Var
100	-2.0907e-1	5.7547e-2	2.1685e-1	3.2270e-2
400	-1.1515e-1	5.2057e-2	1.2637e-1	7.1511e-2
1000	-6.2147e-2	2.5778e-2	6.7281e-2	1.1333e-1

Table 4. *G*1 parameters center point values of lid driven cavity with velocity magnitude variance from [16].
***Indicates fatal instability.**

Re	**Present Work**			
	u_x	u_y	$\|\|\boldsymbol{u}\|\|$	% Var
100	-2.0910e-1	5.7534e-2	2.1687e-1	2.3050e-2
400	-1.1514e-1	5.2061e-2	1.2636e-1	6.3351e-2
1000	*	*	*	*

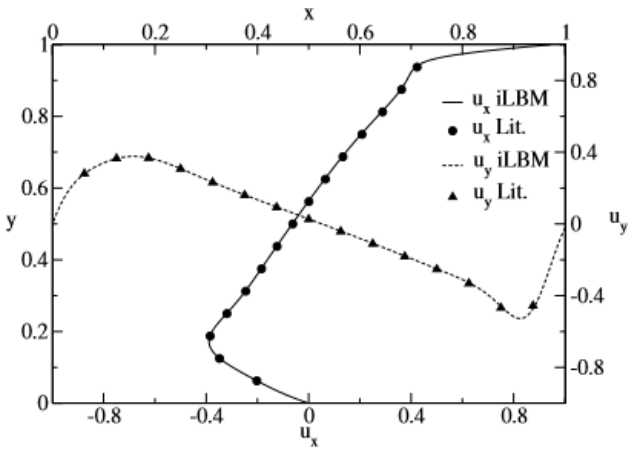

Figure 4. Comparison of *x* and *y* velocities along the centerlines in the lid driven cavity at *Re* 1000 with [16]

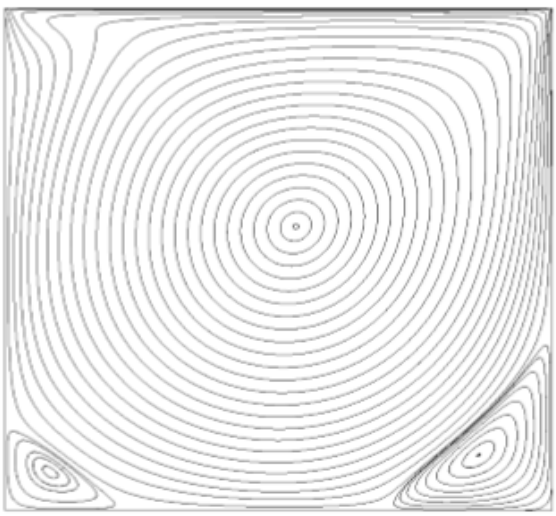

Figure 5. Lid driven cavity flow streamlines at *Re* 1000.

3.3. Womersley flow

Pulsation of flow in a 2D channel is presented here to demonstrate the transient capability of the incompressible LBE derived here. Womersley [17] presented an analytical solution for validation. On a 41x41 grid, a time-dependent pressure difference *dP* is applied. The no slip walls and viscosity resist velocity field changes, but compressibility effects should not. The pressure fluctuation is governed by

$$\frac{\partial P}{\partial x} = \mathrm{Re}\left(Ae^{i\omega t}\right) \tag{29}$$

where $A = dP/L_x$.

The Womersley number describes the relationship of transient inertial forces to viscous force:

$$\alpha = L_y\sqrt{\frac{\omega}{\nu}}, \tag{30}$$

and is necessary in determining the analytical solution:

$$u_x(y,t) = \mathrm{Re}\left(\frac{iAe^{i\omega t}}{\omega}\left(1 - \frac{cos(\lambda(2y/L_y - 1))}{cos\lambda}\right)\right) \tag{31}$$

where $\lambda=\sqrt{-i\alpha^2}$. α is varied in this study by altering ω to show good time-dependent behavior, a major benefit of this approach. Additionally, to display incompressibility, multiple values for *dP* are used.

Figure 6 displays the time dependency of velocity along the *y*-coordinate of the line at $x=L_x/2$ for dP =0.001 and α = 3.98. u_{max} is determined from the Hagen-Poiseuille equation. The analytical results of equation 31 are shown as a solid line, and the numerical results as discrete shapes. Agreement is excellent at each 1/8 fraction of the period past 100000 time steps, and at each point along the centerline. To further validate the method and display its strengths, table 5 shows results as a function of dP, ω (as shown by change in α) compared with He and Luo [5]. Maximum *Ma* is also shown as a potential source of compressibility error amongst numerical errors. As in the transient test of Guo et al. [6], the present fully incompressible scheme results are generally one-half to a full order of magnitude better than [5]. The difference is likely due to the potential for some transient compressibility in [5], since the domain is discretised identically.

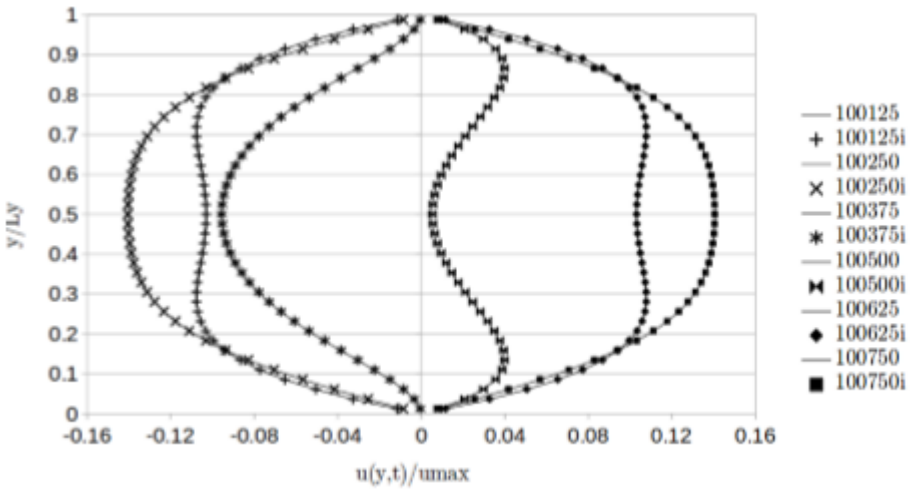

Figure 6. Womersley flow centerline velocity as a function of time and *y*.

Table 5. Womersley flow maximum velocity error at half-*x* from each *y* point, from each *T*/8.

dP	*α*	Ma_{max}	*% Err Present*	*% Err [5]*
0.001	3.98	0.0449	0.0069	0.0182
0.01	3.98	0.449	0.116	0.753
0.001	6.29	0.0163	0.0258	0.247
0.01	6.29	0.163	0.134	1.02

3.4. Backward facing step

The backward facing step combines the inlet/outlet characteristics of the developing channel flow with the vortex generation and shedding nature of the lid driven cavity. Literature provides accurate values for the vortex reattachment point with a variety of *Re*. Here, *Re* = 100, 300, and 800 are simulated with grids 492x50, 892x90, 4002x200, respectively. Convergence is taken to RMS 1e-9. Agreement with the work of Erturk [18] for an expansion ratio of 2.0 is excellent, as seen in table 6.

Table 6. Reattachment point for the backward facing step.

Re	**Present Work**	**Reference**	**% Err**
100	2.920	2.922	0.06845
300	6.778	6.751	0.3999
800	11.87	11.83	0.3381

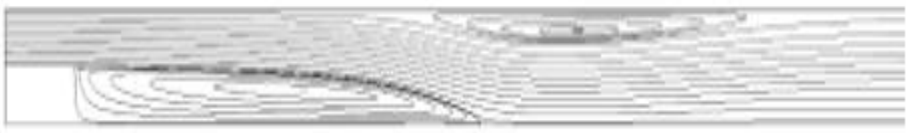

Figure 7. Backward facing step streamlines for *Re* 800.

3.5. 3D lid driven cavity

For 3D verification the procedure laid out in section 2 must be utilized on the D3Q19 lattice (figure 8) with weights

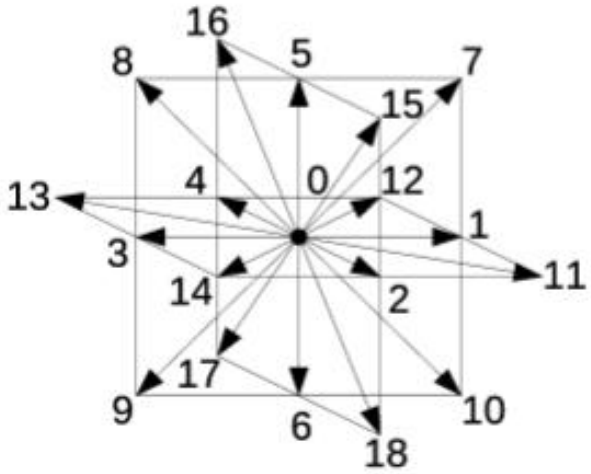

Figure 8. D3Q19 latticce.

$$w_a = \begin{cases} \frac{1}{3} & \text{for} \quad a = 0 \\ \frac{1}{18} & \text{for} \quad a = 1-6 \\ \frac{1}{36} & \text{for} \quad a = 7-18 \end{cases}$$

The resultant EDF with *Constant* = 0 is

$$f_a^{eq} = \begin{cases} -2P/9c^2 + S_a(\boldsymbol{u}), & a = 0 \\ P/54c^2 + S_a(\boldsymbol{u}), & a = 1-6 \\ P/108c^2 + S_a(\boldsymbol{u}), & a = 7-18 \end{cases} \tag{32}$$

where $S_a(\boldsymbol{u})$ is defined in equation 27. Pressure is derived in the same way, and is now

$$P = -\frac{9c^2}{2}\left[\frac{1}{2c^2}(\vec{u}\cdot\vec{u}) + f_0^{eq}\right]. \tag{33}$$

With these parameters definitively resolved, the 3D cubic lid driven is solvable. The cavity is defined with no slip stationary walls except for the top, translating in the $+x$ direction, and 101^3 nodes. For *Re* 100 and 400 the results compare excellently with the incompressible work of Wong and Baker [19]. u_x values along the *z*-direction on a line at x=y=0 are plotted in figures 9 and 10, where the center of the cavity is the datum (0,0,0). Convergencce is taken to RMS 1e-6. Additionally, velocity vectors are plotted on the plane placed at y=0 in figures 11 and 12.

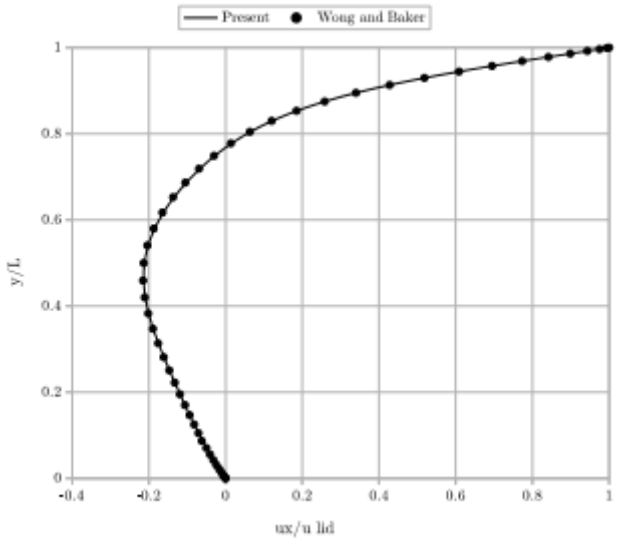

Figure 9. 3D lid driven cavity *Re* 100 *x*-velocity along the line *y*=*x*=0.

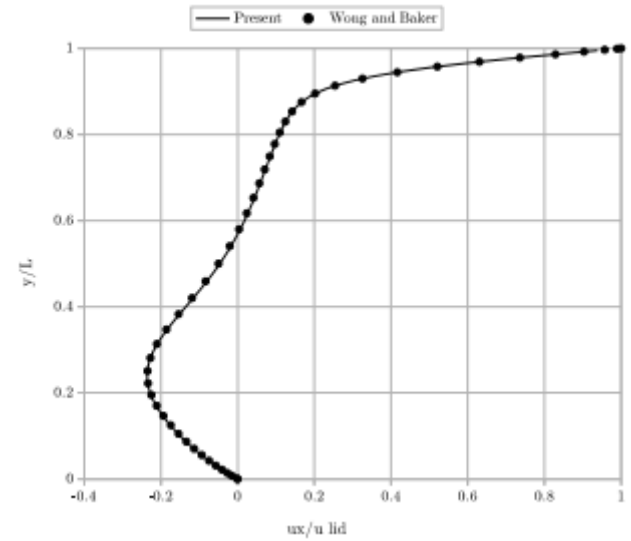

Figure 10. 3D lid driven cavity *Re* 400 *x*-velocity along the line *y*=*x*=0.

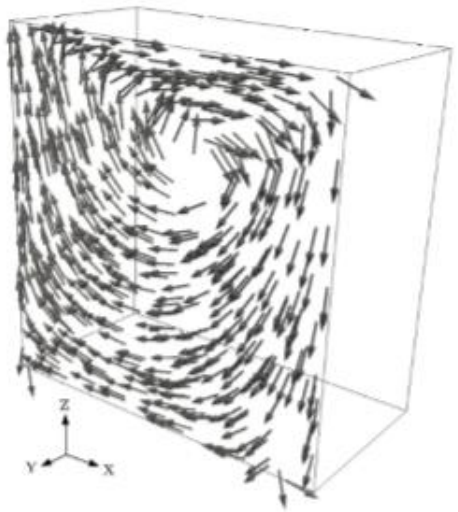

Figure 11. 3D lid driven cavity *Re* 100 velocity at *y*=0.

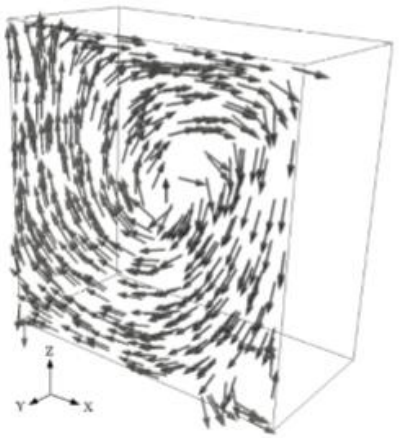

Figure 12. 3D lid driven cavity *Re* 100 velocity at y=0.

IV. CONCLUSIONS

This paper presents an alternative approach to deriving an incompressible lattice Boltzmann equation for steady and unsteady flow simulations by utilizing appropriate ansatzes. The result is a single form of the equilibrium distribution function which recovers the fully incompressible Navier-Stokes equations through the multiscale Chapman-Enskog expansion. The explicit procedure was extended to additional dimensions and lattices. No speed of sound equation is needed in this model, hence no equation of state is needed. Canonical flow simulations yield results in good agreement with the incompressible analytical solutions and literature. The numerical results also show that alternate parameters and forms in previous literature are not as favorable, and that there is an advantage over pseudo-incompressible and compressible forms. The form presented here is thus clarified as necessary for incompressible physics within the lattice Boltzmann method.

Appendix: Chapman-Enskog Expansion for the Incompressible Scheme

From Qian et al. [9] we have an important relationship based on the Knudsen number (*Kn*)

$$\epsilon \equiv Kn \tag{34}$$

Scaling *x*,

$$\epsilon^{-1} x_1 \Rightarrow \frac{\partial}{\partial x} = \epsilon \frac{\partial}{\partial x_1}, \tag{35}$$

and for the same order of magnitude of ε, scaling *t* through the equation

$$\frac{\partial}{\partial t} = \epsilon \frac{\partial}{\partial t_1} + \epsilon^2 \frac{\partial}{\partial t_2}. \tag{36}$$

The slower diffusion time scale is t_2 and the faster convection time scale is t_1.

$$f_a(\boldsymbol{x}, t) = f_a^{(0)}(\boldsymbol{x}, t) + \epsilon f_a^{(1)}(\boldsymbol{x}, t) + \epsilon^2 f_a^{(2)}(\boldsymbol{x}, t) + \mathcal{O}(\epsilon^3), \quad f_a^{(0)} = f_a^{eq}. \tag{37}$$

Performing the perturbation expansion of f_a in terms of ε,

$$\begin{aligned} \frac{1}{\lambda}(f_a^{(0)} - f_a) = & \left(\frac{\partial}{\partial t} + \nabla_{\boldsymbol{x}} \cdot c\boldsymbol{e}_a\right) f_a \\ & + \frac{\Delta t}{2}\left[\frac{\partial}{\partial t}\left(\frac{\partial}{\partial t}\right) + 2\frac{\partial}{\partial t}(\nabla_{\boldsymbol{x}} \cdot c\boldsymbol{e}_a) + (\nabla_{\boldsymbol{x}}\nabla_{\boldsymbol{x}}) : (c\boldsymbol{e}_a c\boldsymbol{e}_a)\right] f_a \\ & + \mathcal{O}(\Delta t^2), \end{aligned} \tag{38}$$

Combining the Taylor Series expansion of f_a with the LBE,

$$\begin{aligned} \frac{1}{\lambda}(f_a^{(0)} - f_a) = & \left(\epsilon \frac{\partial f_a}{\partial t_1} + \epsilon^2 \frac{\partial f_a}{\partial t_2}\right) + \epsilon(\nabla_{x_1} \cdot c\boldsymbol{e}_a) f_a \\ & + \frac{\Delta t}{2}\epsilon^2\left[\frac{\partial^2 f_a}{\partial t_1^2} + 2\frac{\partial}{\partial t_1}(\nabla_{x_1} \cdot c\boldsymbol{e}_a) f_a + (\nabla_{\boldsymbol{x}}\nabla_{\boldsymbol{x}}) : [(c\boldsymbol{e}_a c\boldsymbol{e}_a) f_a]\right] \\ & + \frac{\Delta t}{2}\epsilon^3\left[2\frac{\partial}{\partial t_1}\frac{\partial f_a}{\partial t_2} + 2\frac{\partial}{\partial t_2}(\nabla_{x_1} \cdot c\boldsymbol{e}_a) f_a\right] + \frac{\Delta t}{2}\epsilon^4\left(\frac{\partial^2 f_a}{\partial t_2^2}\right) \\ & + \mathcal{O}(\Delta t^2). \end{aligned} \tag{39}$$

with the aforementioned expansions utilized we obtain

$$\begin{aligned} -\frac{1}{\lambda} f_a^{(1)} &= \frac{\partial f_a^{(0)}}{\partial t_1} + (\nabla_{x_1} \cdot c\boldsymbol{e}_a) f_a^{(0)} \Rightarrow \\ -\frac{1}{\lambda} \sum_a f_a^{(1)} &= \frac{\partial \left(\sum_a f_a^{(0)} \right)}{\partial t_1} + \nabla_{x_1} \cdot \left(\sum_a c\boldsymbol{e}_a f_a^{(0)} \right), \end{aligned} \tag{40}$$

We retain 1st and 2nd order terms of ε for the incompressible case.
Considering terms of 1st order for mass,

$$\sum_{a=0}^{8} f_a^{eq} = \sum_{a=0}^{8} f_a = 0 \tag{41}$$

and with one of the bases (12) for our incompressible scheme,

$$\nabla_{x_1} \cdot \boldsymbol{u} = 0. \tag{42}$$

we arrive at

$$\begin{aligned} -\frac{1}{\lambda} c\boldsymbol{e}_a f_a^{(1)} &= \frac{\partial c\boldsymbol{e}_a f_a^{(0)}}{\partial t_1} + \nabla_{x_1} \cdot c\boldsymbol{e}_a c\boldsymbol{e}_a f_a^{(0)} \Rightarrow \\ -\frac{1}{\lambda} \sum_a c\boldsymbol{e}_a f_a^{(1)} &= \frac{\partial \left(\sum_a c\boldsymbol{e}_a f_a^{(0)} \right)}{\partial t_1} + \nabla_{x_1} \cdot \left(\sum_a c\boldsymbol{e}_a f_a^{(0)} \right), \end{aligned} \tag{43}$$

Looking at 1st order for momentum,

$$\sum_{a=0}^{8} c\boldsymbol{e}_a f_a^{eq} = \sum_{a=0}^{8} c\boldsymbol{e}_a f_a = \boldsymbol{u}, \tag{44}$$

and with the additional basis (13) for our incompressible scheme

$$\frac{\partial \boldsymbol{u}}{\partial t_1} + \nabla_{x_1} \cdot \Pi^{(0)} = 0, \tag{45}$$

we arrive at

$$\Pi^{(0)} (0^{th} \text{ order momentum flux tensor}), \quad \Pi^{(0)} = \sum_a c\boldsymbol{e}_a c\boldsymbol{e}_a f_a^{(0)} = \frac{p}{\rho_0} \boldsymbol{I} + \boldsymbol{u}\boldsymbol{u} \tag{46}$$

Now looking at 2nd order terms in ε for the dissipative terms in the Navier-Stokes equation, for mass conservation,

$$\begin{aligned} -\frac{1}{\lambda} \sum_a f_a^{(2)} = & \left[\frac{\partial}{\partial t_1} \left(\sum_a f_a^{(1)} \right) + \nabla_{x_1} \cdot \left(\sum_a c\boldsymbol{e}_a f_a^{(1)} \right) \right] \\ & + \frac{\partial}{\partial t_2} \left(\sum_a f_a^{(0)} \right) \\ & + \frac{\Delta t}{2} \left[\frac{\partial^2}{\partial t_1^2} \left(\sum_a f_a^{(0)} \right) + 2 \frac{\partial}{\partial t_1} \left(\nabla_{x_1} \cdot \left(\sum_a c\boldsymbol{e}_a f_a^{(0)} \right) \right) \right] \\ & + \frac{\Delta t}{2} \left[(\nabla_{x_1} \nabla_{x_1}) : \left[\sum_a (c\boldsymbol{e}_a c\boldsymbol{e}_a) f_a^{(0)} \right] \right] \end{aligned} \tag{47}$$

Noting that

$$\sum_a f_a^{(G)} = 0, \quad G = 0, 1, 2, \quad \text{and} \quad \sum_a \boldsymbol{e}_a f_a^{(G)} = 0, \quad G = 1, 2, \tag{48}$$

we reduce the 2nd order terms of ε to

$$\frac{\Delta t}{2} \left[2 \frac{\partial}{\partial t_1} \left(\nabla_{x_1} \cdot \sum_a c\boldsymbol{e}_a f_a^{(0)} \right) \right] = \Delta t \frac{\partial}{\partial t_1} \left[\nabla_{x_1} \cdot \boldsymbol{u} \right], \tag{49}$$

$$\frac{\Delta t}{2} (\nabla_{x_1} \nabla_{x_1}) : \left[\sum_a (c\boldsymbol{e}_a c\boldsymbol{e}_a) f_a^{(0)} \right] = \frac{\Delta t}{2} \nabla_{x_1} \cdot \left(-\frac{\partial \boldsymbol{u}}{\partial t_1} \right). \tag{50}$$

Knowing that $\nabla_{x_1} \cdot \boldsymbol{u} = \partial(\nabla_{x_1} \cdot \boldsymbol{u}) = 0$ from above, and using (13) we attain no contribution to the mass equation.

For the contirbution to the momentum equation we have

$$-\frac{1}{\lambda}\sum_a c\boldsymbol{e}_a f_a^{(2)} = \frac{\partial}{\partial t_2}\left(\sum_a c\boldsymbol{e}_a f_a^{(0)}\right) + \left(1-\frac{\Delta t}{2\lambda}\right)\left[\frac{\partial}{\partial t_1}\left(\sum_a c\boldsymbol{e}_a f_a^{(1)}\right) + \nabla_{x_1}\cdot \Pi^{(1)}\right] \quad (51)$$

And similarly to the 0th order momentum flux tensor, the 1st order momentum flux tensor, which for small *Ma*, can be expanded as

$$\begin{aligned} \Pi^{(1)} &= \sum_a c^2 \boldsymbol{e}_a \boldsymbol{e}_a f_a^{(1)} \approx -\lambda\left(\frac{c^2}{3}\right)\left[\nabla_{x_1}\boldsymbol{u} + (\nabla_{x_1}\boldsymbol{u})^T\right] \Rightarrow \\ 0 &= \frac{\partial \boldsymbol{u}}{\partial t_2} - \nu\left[\nabla_{x_1}\cdot\left[\nabla_{x_1}\boldsymbol{u} + (\nabla_{x_1}\boldsymbol{u})^T\right]\right], \quad \nu = \left(\frac{c^2}{3}\right)\left(\tau - \frac{1}{2}\right)\delta t \end{aligned} \quad (52)$$

Studying terms of 1st order in ε, and reversing our scaling of x, we recover the incompressible mass conservation equation

$$\nabla \cdot \boldsymbol{u} = 0 \quad (53)$$

Studying terms of 1st and 2nd order in ε, recalling our momentum flux tensors, and reversing the scaling of t we recover the incompressible momentum equation

$$\begin{aligned} &\frac{\partial \boldsymbol{u}}{\partial t} + \nabla\cdot\Pi^{(0)} = \nu\nabla\cdot\Pi^{(1)} \Rightarrow \\ &\frac{\partial \boldsymbol{u}}{\partial t} + \nabla\cdot(\boldsymbol{u}\boldsymbol{u}) = -\frac{1}{\rho_0}\nabla p + \nu\nabla^2\boldsymbol{u} \end{aligned} \quad (54)$$

REFERENCES

[1]. He, X., Doolen, G. and Clark, T. (2002) 'Comparison of the lattice Boltzmann method and the artificial compressibility method for Navier-Stokes equations', *Journal of Computational Physics*, Vol. 179, No. 2, pp.439–451.

[2]. Zou, Q., Hou, S., Chen, S. and Doolen, G. (1995) 'An improved incompressible lattice Boltzmann model for time-independent steady flows', *Journal of Statistical Physics*, Vol. 81, No. 1, pp.35–48.

[3]. Lin, Z., Fang, H. and Tao, R. (1996) 'Improved lattice Boltzmann model for incompressible two-dimensional steady flows', *Physical Review E*, Vol. 54, pp.6323–6330.

[4]. Chen, Y. and Ohashi, H. (1997) 'Lattice-BGK methods for simulating incompressible fluid flows', *International Journal of Modern Physics C*, Vol. 8, No. 4, pp.793–803.

[5]. He, X. and Luo, L. (1997) 'Lattice Boltzmann model for incompressible Navier-Stokes equation', *Journal of Statistical Physics*, Vol. 88, No. 3, pp.927–944.

[6]. Guo, Z., Shi, B. and Wang, N. (2000) 'Lattice BGK model for incompressible Navier-Stokes equation', *Journal of Computational Physics*, Vol. 165, No. 1, pp.288–306.

[7]. Banda, M.K., Yong, W.A. and Klar, A. (2006) 'A stability notion for lattice Boltzmann equations', *SIAM Journal of Scientific Computing*, Vol. 27, No. 6, pp.2098–2111.

[8]. Shi, B., He, N. and Wang, N. (2005) 'A unified thermal lattice BGK model for Boussinesq equations', *Progress in Computational Fluid Dynamics, An International Journal*, Vol. 5, No. 1-2, pp.50–64.

[9]. Qian, Y., d'Humieres, D. and Lallemand, P. (1992) 'Lattice BGK models for Navier-Stokes equation', *Europhysics Letters*, Vol. 17, No. 6, pp.479–484.

[10]. He, X., Zou, Q., Luo, L. and Dembo, M. (1997) 'Analytic solutions of simple flow and analysis of non-slip boundary conditions for the lattice Boltzmann BGK model', *Journal of Statistical Physics*, Vol. 87, No. 1, pp.115–136.

[11]. Ladd, A. (1994) 'Numerical simulations of particulate suspensions via a discretized Boltzmann equation. Part I. Theoretical foundation', *Journal of Fluid Mechanics*, Vol. 271, pp.285–310.

[12]. Chen, Y., Martinez, D. and Mei, R. (1996) 'On boundary conditions in lattice Boltzmann methods', *Physics of Fluids*, Vol. 8, pp.2527–2531.

[13]. White, F.M. (2005) *Viscous Fluid Flow; 3rd Edition*, New York City:McGraw-Hill.

[14]. Meng, J. and Zhang, Y. (2011) 'Accuracy analysis of high-order lattice Boltzmann models for rarefied gas flows', *Journal of Computational Physics*, Vol. 230, No. 3, pp.835–849.

[15]. Guo, Z., Zhao, T. and Shi, Y. (2004) 'Preconditioned lattice-Boltzmann method for steady flows', *Physical Review E*, Vol. 70, pp.066706.

[16]. Marchi, C.H., Suero, R. and Araki, L.K. (2009) 'The lid-driven cavity flow: Numerical solution with a 1024 x 1024 grid', *Journal of the Brazilian Society of Mechanical Science & Engineering*, Vol. 31, No. 3, pp.186–198.

[17]. Womersley, J.R. (1955) 'Method for the calculation of velocity, rate of flow and viscous drag in arteries when the pressure gradient is known', *Journal of Physiology*, Vol. 127, No. 3, pp.553–563.

[18]. Erturk, E. (2008) 'Numerical solutions of the 2-D steady incompressible flow over a backward-facing step, Part I: High Reynolds number solutions', *Computers & Fluids*, Vol. 37, No. 6, pp.633–655.

[19]. Wong, K.L. and Baker, A.J. (2002) 'A 3D incompressible Navier-Stokes velocity-vorticity weak form finite element algorithm', *International Journal of Numerical Methods for Fluids*, Vol. 38, No. 2, pp.99–123.